Pressure-induced circumferential and longitudinal deformations of tracheal tubes in the American cockroach

Matthew R. Webster[1], Roshelle S. Wijeratne[1], John J. Socha[2], and Raffaella De Vita[1,*]

[1]STRETCH Lab, Department of Mechanical Engineering, Virginia Tech, Blacksburg, VA, 24061
[2]Department of Mechanical Engineering, Virginia Tech, Blacksburg, VA, 24061

[*]Author for correspondence: (Raffaella De Vita; devita@vt.edu)

ABSTRACT

Insects exchange gases through a complex internal network of tubes known as tracheae, which deliver oxygen directly to tissues and remove carbon dioxide. In some species, these tracheal tubes undergo active compression, periodically collapsing and reinflating to facilitate internal airflow. The mechanical behavior of the tracheal system is governed by its structural design, which in turn influences its physiological role in respiration. Despite the critical importance of tracheal material properties in insect respiratory function, there are relatively few published studies that characterize their uniaxial tensile behavior. In this study, we present new experimental methods for measuring the pressure-induced biaxial deformations of tracheal tubes isolated from the American cockroach (*Periplaneta americana*). To this end, an inflation–extension testing device was built to subject tracheae to increasing internal pressures (0-6 kPa) and axial displacements (0-0.2 mm). Local circumferential and longitudinal stretches were quantified using non-contact strain measurement techniques. In most cases, circumferential stretches increased nonlinearly with applied pressure at any axial displacements, while longitudinal stretches changed minimally. This behavior likely reflects the combined influence of structural anisotropy, mechanical coupling, and geometric constraints. The observed deformations highlighted the mechanical sophistication of insect tracheae. They underscored the importance of integrating geometry and microstructure to understand how these structures resist collapse, enable gas exchange, and adapt to mechanical demands.

Journal of Experimental Biology • Accepted manuscript

Keywords: insect tracheae, American cockroach, inflation-extension testing, mechanical properties, cuticle biomechanics

INTRODUCTION

Insects deliver oxygen to every cell in their body through an intricate network of flexible tracheal tubes (Harrison, 2009). In many species, large deformations of the tracheal system generate advective airflow (Westneat et al., 2003, Westneat et al., 2008, Socha et al., 2008, Greenlee et al., 2013, Hochgraf et al., 2018), a mechanism essential for meeting the high metabolic demands of activities like flight (Miller, 1966). This unique respiratory architecture not only supports the highest mass-specific metabolic rates in the animal kingdom (Suarez, 2000), but also allows insects to modulate oxygen delivery rapidly through tracheal compression, with minimal active control (Harrison, 1997, Weis-Fogh, 1967). As a result, insects can achieve dynamic changes in oxygen uptake that far exceed those of vertebrates (Suarez, 2000). Effective respiration in insects relies on a flexible and dynamic network of tracheal tubes. The ability of this system to generate airflow, particularly through large deformations, depends on the microstructure of the tracheae.

Insect tracheal structures are built from cuticle, a composite biological material whose properties are finely tuned to meet diverse functional demands. Although composed of relatively few basic constituents (namely chitin, heavy metals, lipids, and protein), the cuticle exhibits a remarkable range of mechanical behaviors depending on its microstructural arrangement and environmental conditions (Vincent and Wegst, 2004). The cuticular structure of insect tracheae combines flexibility with strength, allowing the walls to deform as needed while maintaining support for respiration. In the primary thoracic tracheae of the American cockroach (*Periplaneta americana*), this balance is achieved through a wall dominated by circumferentially oriented taenidia, which form continuous helical ridges and constitute more than 80% of the wall thickness. These taenidia often bifurcate in a non-random pattern, suggesting a structured reinforcement network that may influence local mechanical behavior during deformation. Adjacent to the taenidia, fine fibers aligned along the longitudinal direction interconnect successive rings, likely constraining longitudinal deformation and maintaining wall integrity

under extension. Beneath these layers, the endocuticle contains a meshwork of fibers embedded within a protein matrix (Webster et al., 2015a). This hierarchical organization, characterized by circumferential taenidial reinforcement, longitudinal interconnections, and an underlying fibrous matrix, is fundamentally responsible for the mechanical response of the tracheal wall.

The primary thoracic tracheae of the American cockroach have a highly organized, composite microstructure that reflects their dual demands for flexibility and structural stability. The tracheal wall is dominated by circumferentially oriented taenidia, which form continuous helical ridges and constitute more than 80% of the wall thickness. These taenidia often bifurcate in a non-random pattern, suggesting a structured reinforcement network that may influence local mechanical behavior during deformation. Adjacent to the taenidia, fine fibers aligned along the longitudinal direction interconnect successive rings, likely constraining longitudinal deformation and maintaining wall integrity under extension. Beneath these layers, the endocuticle contains a meshwork of fibers embedded within the matrix (Webster et al., 2015a). This hierarchical organization (circumferential taenidial reinforcement, longitudinal interconnections, and an underlying fibrous matrix) is responsible for the mechanical response of the tracheal wall.

The mechanical properties of many types of cuticle from a wide range of insect species have been examined through uniaxial tests. In their pioneering work, Jensen and Weis-Fogh used a custom-built uniaxial testing system to examine the static and dynamic properties of the hard and soft cuticles of locusts (Jensen and Weis-Fogh, 1962). Hepburn and colleagues used similar methods to study the properties of extracted chitin lamellae from the cuticle of beetles (Hepburn, 1972), and the hard and soft cuticles of locusts, silkworms, and beetles (Hepburn and Chandler, 1976a). By performing uniaxial ring-tests, Reynolds studied the time-varying properties of the expandable cuticle of ticks (Reynolds, 1975). More recent investigations include the study of the properties of various sections of the hind wing of the desert locust (Smith et al., 2000), the integument (Lin et al., 2009) and musculature (Dorfmann et al., 2007, Dorfmann et al., 2008) of caterpillars, the neck joint of ants (Nguyen et al., 2014), and female reproductive tract of a beetle (Matsumura et al., 2021). Indentation methods have also been employed to evaluate insect cuticle, but they primarily measure localized stiffness or hardness under compressive loading and do not capture how the material deforms under distributed tensile or pressure-driven loads typical of physiological conditions (Siamantouras et al., 2022).

To our knowledge, the only data on the material properties of the tracheal cuticle have been published in our previous studies (Webster et al., 2011, Becker et al., 2015). In these studies, the cuticle of the primary thoracic tracheal trunks of the American cockroach (*Periplaneta americana*) was tested in the circumferential direction by means of uniaxial ring tests. Our findings revealed that the tracheae are highly nonlinear, elastic materials (Webster et al., 2011). A large variation in the material properties of ring specimens was also observed, but such variation was found to decrease significantly for ring specimens isolated from the same trachea (Becker et al., 2015). While these uniaxial tests provided the first measurements of tracheal material behavior, they characterized deformation only in a single direction (circumferential), under uniform tension. In contrast, the native trachea is simultaneously subjected to pressures and forces acting in multiple directions–internal pressure generates both circumferential and longitudinal stresses, while additional longitudinal loading arises from body and respiratory motion. Biaxial testing captures this coupled response by applying controlled loads in two directions at once, thereby revealing how deformation in one direction influences the other. Such coupling cannot be inferred from uniaxial data alone, particularly for anisotropic composite structures such as the tracheal wall. To date, there is no published study on the mechanical properties of any form of insect cuticle using biaxial tests. The lack of such data on the insect cuticle may stem from difficulties involved with handling and testing minute and fragile biological specimens such as tracheae.

The tubular geometry of the tracheae lends itself to inflation-extension biaxial tests, whereby a specimen is inflated while simultaneously being extended along its longitudinal axis. This testing method, which has been used to study the nonlinear-elastic properties of vulcanized rubber (Vangerko and Treloar, 1978, Haughton and Ogden, 1979), mammalian cardiovascular tissue (Takamizawa and Hayashi, 1987, Holzapfel and Weizsäcker, 1998, Wicker et al., 2008), and flexible matrix composites (Shan et al., 2006), alleviates some of the inherent difficulties of planar biaxial testing (e.g., preventing slippage at grips and avoiding edge effects) and re-creates more physiologically-relevant loading conditions. It enables tubular specimens to be gripped to the testing system via their two ends while still being deformed biaxially. More specifically, the mechanical behavior of a material in two perpendicular directions, the longitudinal and circumferential directions in the case of insect tracheal tubes, can be characterized by performing

these tests. However, the small size of the tracheae requires the development of a custom-built testing system with new methods for specimen gripping and for the analysis of the resulting deformation.

Here, we addressed the question, What is the mechanical behavior of insect tracheal tubes under biaxial loading conditions? Specifically, this study examined the biaxial nonlinear elastic response of the primary thoracic tracheal tubes of the American cockroach (*Periplaneta americana*). These larger tracheal tubes contribute primarily to advective airflow within the respiratory network, whereas diffusion dominates in the finer tracheoles. Beyond their physiological relevance, they were also selected because their size facilitates isolation, mounting, and mechanical testing under controlled conditions. Toward this end, *ex vivo* inflation-extension tests were performed on these tubes using a custom-built testing system. Our protocol consisted of three inflation-extension tests, each performed at a different fixed displacement while incrementally increasing internal pressure. These tests simulate the combined internal pressurization and displacements that insect tracheae undergo during activities such as walking, flying, or abdominal pumping. The local deformation of the tracheal tubes in the circumferential and longitudinal directions was computed using a non-contact strain method known as the digital image correlation (DIC) method. This study represents a significant first step toward the characterization of biaxial elastic properties of the insect tracheae and other chitinous insect cuticle. Our findings advance our limited knowledge of how structural and material specializations in insect tracheae support respiratory function, offering insight into the evolutionary design of efficient, deformable biological conduits.

EXPERIMENTAL METHODS

Specimen Preparation

Thirteen adult male American cockroaches (*Periplaneta americana*) were obtained from the Department of Entomology at Virginia Tech (mass: 0.846 $\pm$ 0.070 g; body length: 33.80 $\pm$ 1.17 mm; mean $\pm$ S.D.). The insects were housed under ambient laboratory conditions (21–23 $^{\circ}$C) and provided with food and water *ad libitum*. Prior to mechanical testing, insects

were euthanized using ethyl acetate fumes. Within 12 hours of sacrifice, the primary thoracic tracheae were carefully excised, as illustrated in Fig. 1 and described in previous studies (Webster et al., 2011, Becker et al., 2015). These tracheae were chosen for their large size, their ability to undergo in situ compression, and to enable direct comparison with prior uniaxial data. Each trachea was trimmed to isolate a segment with approximately uniform geometry and tested immediately after dissection. A total of 21 tracheal tubes (11 right dorsal, 10 left dorsal) were successfully tested and analyzed. The tested tracheal tubes had a mean length of 2.81 ± 0.30 mm, a mean circumference of 2.33 ± 0.16 mm, and a mean thickness of 6.7 ± 0.5 μm. However, due to irregular or highly variable deformation behaviors in 11 specimens, only 10 that exhibited consistent trends were selected for further comparison and interpretation.

Each tracheal tube was maintained in insect Ringer's solution (0.75 g NaCl, 0.035 g KCl, 0.021 g $CaCl_2$, in 100 ml distilled water) at room temperature (Williams, 1946). Tube dimensions were measured optically using images captured by a stereo microscope (Stemi-2000C; Carl Zeiss, Jena, Germany) equipped with a digital camera (D5000; Nikon Corporation, Tokyo, Japan). The image scale (pixels to physical units) was calibrated using a 1 mm optical grid. The initial length of each tracheal tube was recorded prior to testing. Specimens were then speckle-coated with black ink using an airbrush (Model G444; Master Airbrush; San Diego, CA) to enable non-contact deformation tracking before mounting on the testing system.

Testing System and Protocol

A custom testing system was developed to perform inflation-extension experiments on insect tracheae (Fig.2A). The setup included a linear actuator (TNa Series Linear Actuator; Zaber Technologies, Vancouver, Canada), a low-capacity load cell (LSB200 Jr. S-Beam Load Cell; Futek Advanced Sensor Technology Inc., Irvine, CA) with a maximum capacity of 0.49 N and an accuracy of ± 740 μN. Internal pressurization was achieved using an aquarium air pump (Topfin AIR-500; Petsmart Inc., Phoenix, AZ), and the internal pressure was monitored using a pressure sensor (Model No. MMG2.5V5P2D0T1A3; Omega Engineering Inc., Stamford, CT), with a measurement range of 0-17.2 kPa (corresponding to an output of 0–2.5 V) and a

resolution of ± 0.018 kPa. Displacement was applied by the actuator at a constant rate of $10\ \mu m\ s^{-1}$, with a minimum step size of 0.28 μm, allowing for precise control of elongation during testing.

Local tissue deformation was recorded using a stereo-camera system composed of two CCD cameras (Stingray F080B; Allied Vision Technologies Inc., Stradtroda, Germany) equipped with telecentric lenses (TechSpec Compact Telecentric Lens; Edmund Optics Inc., Barrington, NJ). Data acquisition and control were managed using a NI-cDAQ 9172 system (National Instruments Corp., Austin, TX). All tests were performed in a custom-built bath to maintain tissue hydration and imaging conditions.

Each tracheal tube was mounted onto the testing system using two 0.5 mm diameter syringe tips. Paraffin wax was applied to each tip and melted using a soldering iron to create an adhesive bead. One end of the tracheal tube was sealed to the syringe tip connected to both the linear actuator and the air pump. The actuator was then used to position the opposite end of the tube onto the second syringe tip, which was connected to the load cell, and the wax was remelted to secure the attachment (Fig.2B). The tubes were positioned with the dorsal side facing the cameras (Fig.2C). Immediately following mounting, insect Ringer's solution was added to the custom-built bath, and the specimen was allowed to hydrate for at least 5 minutes prior to testing.

Once mounted and hydrated, each tracheal tube was axially preloaded to approximately 0.5 mN in tension and allowed to rest for an additional 5 minutes before inflation testing. This nominal preload, applied after submersion, was intended to remove slack and standardize the initial configuration. Although the applied force approached the lower resolution limit of the load cell and may have included minor hydrostatic effects, it was not used in any quantitative analysis. Because insect cuticle is susceptible to micro-scale damage during cyclic loading (Hepburn and Chandler, 1976b), no preconditioning protocol was employed to avoid compromising tissue integrity.

Three inflation tests were conducted on each tracheal specimen at axial displacements δ_z of 0.0, 0.1, and 0.2 mm (Fig.4). At each displacement, the specimen was allowed to relax for approximately 30 s before being internally pressurized to a maximum of 6 kPa. Preliminary tests indicated that specimens could be safely pressurized up to 6 kPa without structural damage. This value was therefore adopted as the upper pressure limit, as it also corresponds to hemolymph pressures observed in vivo (e.g., (Pendar et al., 2019)). Air was delivered into the tube at an approximate flow rate of 16.67 $cm^3\ s^{-1}$, and the pressurization rate was tuned by adjusting the volume of a reservoir placed in-line between the air pump and the syringe tip. This setup produced an effective pressurization rate of approximately 0.035 kPa s^{-1}.

The local deformation of the tracheal tube throughout testing was measured optically using a stereo-camera system equipped with macro lenses (Fig.3). The two monochrome cameras were positioned in the same vertical plane, offset by approximately 24° relative to each other, and mounted on a two-axis micrometer stage (Thorlabs Inc.; Newton, NJ) for precise alignment. Each camera captured 1032×778 pixel images of the tracheal surface synchronously with pressure data acquisition. The pixel size was $\pm 1.11\ \mu$m, determined by the pixel dimensions of the sensors and the lens magnification.

The optical system was calibrated following each test using images of a grid distortion target (Thor Labs Grid Distortion Target; Thorlabs Inc., Newton, NJ) acquired at multiple distances from the stereo-camera system. Calibration was performed by implementing the normalized direct linear transformation method (Gorpas et al., 2007, Hartley and Zisserman, 2000), resulting in a mean depth measurement error of $3.23 \pm 0.64\ \mu$m.

To quantify specimen local deformation, the three-dimensional coordinates of a virtual rectangular grid of surface points on the tracheal tube, in the central region, away from the syringe tips (Fig.2C), were computed at each time step using three-dimensional DIC. This method extends traditional DIC by applying cross-correlation to a speckle pattern on the specimen surface, first to identify matching features in stereo image pairs (stereo matching), and subsequently to track their displacement over time (temporal matching) (Garcia et al., 2002).

A MATLAB-based software package originally developed for two-dimensional DIC (Eberl et al) was modified to implement three-dimensional DIC. The surface profile of the tracheal tube was reconstructed from synchronized image pairs using the normalized direct linear transformation calibration data. Longitudinal stretch, λ_z, was computed from the displacement of grid lines along the longitudinal direction as: $\lambda_z = l(t) / l(0)$, where $l(0)$ and $l(t)$ represent the average lengths of 10 to 12 grid lines at the initial time ($t = 0$, at $\delta_z = 0$) and at any subsequent time t, respectively. The circumferential stretch was computed as $\lambda_\theta = s(t) / s(0)$, where $s(0)$ and $s(t)$ were the average arc-lengths of approximately 10 to 12 grid curves along the circumferential direction at $t = 0$ (when $\delta_z = 0$) and at any subsequent time t, respectively. The local radius of curvature, ρ, at each time for each circumferential grid curve located at the same longitudinal location was computed from the coordinates of three points located at the two ends and at the center of such curve (Fig. 2C). Then the local radius of curvature of the tracheal tube at any time was computed as the average of the radii of curvature computed from the 10 to 12 circumferential grid curves (Fig.2C).

Data were collected using a data acquisition (DAQ) module at a sampling rate of 10 Hz. Both test control and data acquisition were managed through a custom LabVIEW program (LabVIEW 2009; National Instruments Corp., Austin, TX).

RESULTS

The mechanical response of the tracheal tubes was clearly dependent on the level of axial displacement (δ_z) applied prior to inflation. A predominant characteristic mechanical behavior was identified in $n = 10$ specimens. Detailed results from one of these representative specimens at the three axial displacements ($\delta_z = 0, 0.1, 0.2$ mm) are shown in Fig. 5. In addition to the monotonically increasing pressure–circumferential stretch (λ_θ) and pressure–longitudinal stretch (λ_z) relationships (Figs. 5A,B), Fig. 5C illustrates the coupling between λ_θ and λ_z, while Fig. 5D shows how the local radius of curvature changes as the pressure increased. The data

indicated that at $\delta_z = 0.0$ mm, deformation was greatest in both the circumferential and longitudinal directions. At higher axial displacement, deformation in both directions increased, with a disproportionately greater increase in the circumferential direction (Figs. 5A,B).

At zero longitudinal displacement ($\delta_z = 0.0$ mm), the $\lambda_z - \lambda_\theta$ curves were noticeably nonlinear, whereas at non-zero displacements ($\delta_z = 0.1$ and 0.2 mm) they became more linear. In all cases, longitudinal stretch increased with circumferential stretch, but at the larger axial displacements, λ_θ approached its maximum value while λ_z increased only slightly. This indicates that the deformation occurred predominantly in the circumferential direction, as seen in the steep slopes of the $\lambda_z - \lambda_\theta$ curves for $\delta_z = 0.1$ and 0.2 mm (red curves in Fig. 5C). Because the stretch values were computed relative to the reference configuration, i.e. at $\delta_z = 0$, when the tube was axially displaced to $\delta_z = 0.1$ or 0.2 mm, the dorsal surface contracted slightly along the circumferential direction and became longer in the longitudinal direction. For this reason, the circumferential stretch measured at these pre-stretched states was less than 1, and the longitudinal stretch was greater than 1.

The radius of (circumferential) curvature of the tracheal surface was found to decrease as the internal pressure increased during the inflation-extension tests at all axial displacements ($\delta_z = 0.0$, 0.1, and 0.2 mm) (Fig. 5D). The highest change in the radius of curvature occurred when the tracheal tube was under an internal pressure between 0 kPa and 3 kPa. As the internal pressure reached values that were approximately higher than 4 kPa, the radius of curvature of the tracheal surface did not change significantly (Fig.5D). Moreover, increasing the axial displacement δ_z from 0.0 mm to 0.2 mm caused a local increase in the radius of curvature due to local flattening of the dorsal surface of the tracheal tube. Because the tubes were mounted with the dorsal (flatter) side facing the cameras, the measured curvature reflects this local region of the cross-section rather than the global shape of the tube. With increasing internal pressure, the cross-section became more circular and the dorsal wall curved more tightly, resulting in a decrease in the locally measured radius of curvature. This transition from a flattened profile (larger radius of curvature) to a more circular shape (smaller radius of curvature) suggests that pressurization promotes a geometry that more evenly distributes internal pressure.

Data for all tested specimens ($n=10$) are reported in Figs. 6-7. The mean ($\pm$ standard error of the mean, S.E.M.) values of both λ_z and λ_θ are also reported at 0.25 kPa increments of internal pressure for each axial displacement ($\delta_z = 0.0$, 0.1, and 0.2 mm). The average behavior is qualitatively similar to the behavior of the representative specimen shown in Fig. 5. The circumferential stretches increased exponentially at low pressures and roughly linearly at high pressures for most of these specimens (specimens 3-10, Fig.6). As the axial displacement δ_z increased from 0.0 to 0.2 mm, the value of λ_θ at zero-pressure decreased and the specimens appeared to stiffen at lower stretches (Fig.6A-C). The pressure versus the longitudinal stretch λ_z curves were nonlinear at low longitudinal stretches for several of these specimens (Fig.7A). But, as δ_z increased, the nonlinearity decreased and the slope of the pressure versus λ_z curves increased. For some specimens, a critical level of elongation was reached beyond which the tracheae became shorter ($\lambda_z < 1$), at least locally, when pressurized rather than elongating (see, for example, specimen 8 in Fig. 7A and specimens 4, 7, and 8 in Fig. 7B-C).

The remaining specimens ($n=11$) exhibited other patterns of behavior. Some specimens appeared to be compressed in the circumferential direction as the internal pressure increased; representative data for one are shown in Fig. 8. Often, but not always, the circumferential stretch decreased exponentially with the internal pressure. Within this set of specimens, there was large variability in the effect of increased axial displacement on the elastic response of the material. In some cases, increasing the axial displacement caused an increase in the circumferential stretch at the zero pressure value (Fig. 8A), while in other cases it caused a decrease in such circumferential stretch. Some specimens showed an increase in the slope of the linear region of the pressure versus circumferential stretch curves, as δ_z increased, while others showed little or no change in such slope. The internal pressure versus longitudinal stretch curve showed a stiffening response that was similar to that seen for the first group of specimens (Fig. 5B versus Fig. 8B). There was a nonlinear coupling between the circumferential stretch and the longitudinal stretch, but with a trend that was often opposite to that observed for the first group of specimens (Fig. 5C versus Fig. 8C). Specifically, as the longitudinal stretch increased, the circumferential stretch decreased (Fig. 8C). The radius of curvature versus internal pressure curves for these specimens increased as δ_z increased, and decreased as the pressure increased.

The most significant changes in curvature occurred as the pressure rose from 0 kPa to roughly 3 kPa (Fig. 8D), a trend also observed for the representative specimen in Fig. 5D.

DISCUSSION

In this study, we conducted *ex vivo* inflation–extension experiments to characterize how the tracheae of the American cockroach deform under controlled internal pressure and axial displacement. These experiments were technically challenging due to the small size and fragile nature of the tracheal tubes, requiring careful mounting and precise deformation tracking. Despite these difficulties, we successfully applied biaxial loading and directly measured local deformations using high-resolution optical methods. Under these conditions, the tracheae exhibited highly nonlinear behavior, confirming the nonlinearities observed in our previous ring tests (Webster et al., 2011, Becker et al., 2015). The hierarchical organization of the insect tracheae likely contributes to the pressure-dependent stiffening and directional stretch responses observed in our experiments.

We identified a dominant deformation behavior in which the mode of stretch depended strongly on the level of axial displacement (Fig. 5). At zero axial displacement ($\delta_z = 0.0$ mm), both circumferential and longitudinal stretches increased greatly with pressure, indicating that the tracheal wall deformed in both directions. At higher fixed elongations ($\delta_z = 0.1$ and 0.2 mm), however, the same pressure increase produced much larger changes in circumferential stretches while longitudinal stretches changed only slightly. The reduced changes in longitudinal stretch at higher δ_z likely reflect the fact that much of the available longitudinal compliance was already taken up by the initial axial displacement, leaving the tracheal wall to accommodate additional pressurization primarily through circumferential expansion. Such deformation behavior may help insect tracheae preserve longitudinal stability and maintain airway patency during normal physiological activities, such as flight and locomotion, that entail simultaneous internal pressurization and axial displacement. By accommodating body movements through controlled geometric changes rather than large material strains, the tracheae can redistribute wall stresses and undergo reversible deformation, maintaining efficiency across loading states.

The tracheal tubes used in this study were carefully selected to exhibit a relatively uniform cylindrical geometry. To minimize boundary effects, deformation was measured locally within a central region of each specimen, sufficiently distant from the clamping syringe tips. Despite these precautions, inhomogeneous deformation was frequently observed, primarily due to local bending caused by geometric irregularities inherent to the tracheal tubes. These variations underscore the importance of using three-dimensional DIC, which enabled spatially resolved strain measurements and revealed how minor geometric differences influenced local mechanical responses.

Locally, the tracheal cross-section became more circular under internal pressurization, reflecting radial expansion, whereas the application of axial displacement induced a flattening of the cross-section (Fig. 5D). This tendency of elliptical cross-sections to round under internal pressure has been previously observed in flexible cylindrical structures and can result in inhomogeneous deformation fields; some regions experience local compression while others undergo stretching (Kresch, 1977). The local flattening with axial displacement is likely due to natural variations in cross-sectional geometry along the tracheal length. In this study, tracheal tubes were mounted in the inflation–extension apparatus with the dorsal side facing the cameras, ensuring that the same anatomical region was imaged in each specimen and that their cylindrical geometry was preserved as much as possible. Nevertheless, the cross-section was frequently flatter on the ventral side in the central area. Importantly, our measurements focused on local deformation and did not capture cross-sectional shape changes along the full tracheal length. For tracheae with more irregular geometry, the mechanical response to pressure and axial displacement was influenced not only by material behavior but also by spatial variation in cross-sectional shape. The difficulty in isolating the intrinsic material properties of insect cuticle from the structural behavior of the body parts it forms has been well-documented in the literature (Stamm et al., 2021), with similar problems reported for structures such as wings, legs, and exoskeletal joints.

During testing, some tracheal tubes exhibited bending due to the natural curvature of their longitudinal axis (Fig. 3). In several cases, this curvature became more pronounced upon inflation. Misalignment during specimen mounting, particularly at the grips, further exacerbated changes in longitudinal curvature during testing. Although specimens with clearly visible

misalignment were excluded from the dataset, minor deviations may still have been present in the analyzed specimens. These geometric irregularities posed practical challenges in applying uniform, controlled deformations to the tracheae. They demonstrated the role that geometry plays in determining the mechanical response of tracheal tubes under complex loading conditions. Variability among specimens may also reflect compositional inhomogeneities within the tracheal wall. While chitin fibers are the primary structural component, it is possible that some species of insects incorporate varying amounts of resilin–a rubber-like protein known for its exceptional elasticity and energy return (Weis-Fogh, 1960). Resilin has been identified in several insect structures, including wing veins, joint membranes, mouthparts, and reproductive tissues. Emerging imaging methods, such as fluorescence microscopy and confocal laser scanning microscopy, could be used to assess the presence or distribution of resilin within the tracheal system (Appel et al., 2024).

In our previous analysis of the microstructure of tracheal tubes (Webster et al., 2015a), we identified regions in which the taenidia exhibited irregular arrangements. It is possible that these local structural variations, such as taenidial branching or discontinuities, dictate the mechanical coupling between longitudinal and circumferential stretches observed during inflation-extension testing (Figs. 5C and 8C). The observed circumferential deformation likely involves stretching of the taenidia, whereas longitudinal deformation may be mediated by mechanisms such as tissue unfolding or delamination between the taenidia and the surrounding cuticular layers (i.e., the endocuticle and epicuticle). Because the microstructure of the tested specimens was not examined pre- or post-deformation in this study, future analyses that directly link mechanical testing with high-resolution imaging will be essential to elucidate the micro-scale mechanisms underlying tracheal deformation. Such investigations could clarify the structural basis for the coupling between circumferential and longitudinal stretch responses.

Despite the limitations that are involved with the assessment of the elastic response of small and geometrically irregular insect tracheal tubes, this study advances our understanding of the biaxial mechanical behavior of the tracheae in the American cockroach. For the first time, we were able to observe and quantify the local deformations of the tracheae under combined pressure and axial displacement, the coupling between the circumferential and longitudinal deformations, and the change in curvature. Using the experimental methods described here and

the new knowledge regarding the mechanical response of the tracheae, it will soon be possible to simulate the elastic response of the tracheal networks of insects under their complex *in vivo* loading and boundary conditions.

As a first step toward such simulations, we implemented a Holzapfel–Gasser–Ogden (HGO) model (Holzapfel et al., 2000) which consisted of an isotropic matrix reinforced by three fiber families, two fixed along the circumferential and longitudinal directions, and one oblique family whose orientation was determined through model fitting (Webster et al., 2015b). Data from our inflation–extension tests ($n=10$) were used to compute circumferential and longitudinal stresses based on equilibrium relations for a thin-walled cylindrical tube in the deformed configuration. In this modeling framework, two parameters are used for each fiber family: k_1 represents the initial fiber stiffness and k_2 the exponential coefficient governing strain stiffening. The fitted parameters indicated a compliant isotropic matrix with shear modulus $\mu_m \approx 0.46\,\text{MPa}$; very stiff circumferential fibers with $k_1 \approx 3.0\,\text{MPa}$ and $k_2 \approx 3200$; more compliant longitudinal fibers with $k_1 \approx 0.10\,\text{MPa}$ and $k_2 \approx 12$; and oblique fibers of intermediate stiffness with $k_1 \approx 2.25\,\text{MPa}$ and $k_2 \approx 510$, oriented at $\alpha \approx 52^\circ$ relative to the longitudinal direction. These results provide quantitative parameters for modeling tracheal wall anisotropy and are consistent with the observed microstructure of the tracheae (Webster et al., 2015a). They show that the wall is markedly stiffer in the circumferential direction under the applied loading conditions, a response attributable to the helical organization of the taenidial rings. This fiber-reinforced architecture strengthens the wall circumferentially, governing its overall mechanical behavior.

Insects experience both supra-ambient (positive) and sub-ambient (negative) intratracheal pressures depending on physiological state and behavior. Positive pressures occur transiently during ventilatory pumping, abdominal compression, or wing-assisted locomotion, when air is actively forced through the tracheal system and the internal pressure exceeds that of the surrounding hemolymph. In contrast, negative pressures arise when the internal air pressure drops below the external pressure, such as during the closed-spiracle phase of gas exchange, hemolymph pulsations, or immersion-related hydrostatic compression, leading to inward deformation or partial collapse of the tracheal wall. In this study, the tracheae were pressurized from atmospheric pressure (0 kPa) to +6 kPa, representing the expansion phase of the tracheal

loading cycle. This range was selected to capture the material response under controlled outward deformation while maintaining optical stability for DIC imaging. Tests under sub-ambient pressure would more closely represent physiological collapse, but such experiments are more difficult to conduct, as inward motion and early buckling obscure the speckle pattern, preventing reliable strain mapping.

The observed interaction between circumferential and longitudinal deformation, together with changes in curvature, indicates that geometric and material nonlinearities jointly govern the mechanical performance of insect airways. These nonlinear features likely enable the tracheal wall to accommodate complex loading while maintaining structural integrity and reversible deformation. Deforming the wall requires energetic input, but part of this energy may be stored as elastic strain energy and released during recoil, assisting airflow and reducing the energetic cost of ventilation. The tracheal system, therefore, appears tuned to support low-energy respiration through the interplay of active, muscle-driven pressure fluctuations and passive, elastic recoil of the tracheal walls, a combination that may inform biomimetic designs for energy-efficient fluid transport systems (e.g., (Aboelkassem and Staples, 2012), (Chatterjee et al., 2021)). From an engineering perspective, understanding how geometry and material properties interact to enable efficient, reversible deformation in tracheal walls can inform the design of biomimetic or bioinspired flexible tubing systems, such as those used in soft robotics, wearable microfluidics, and tunable ventilation structures, where resilience and compliance must be precisely balanced to achieve reliable and energy-efficient fluid transport (Chatterjee et al., 2021, Ren et al., 2021, Khan and Staples, 2025, Zheng et al., 2025).

CONCLUSION

Despite the challenges associated with experimentally characterizing the deformations of small, geometrically irregular insect tracheal tubes, this study provides the first direct experimental data on the biaxial mechanical behavior of tracheae in the American cockroach. Using inflation-extension tests, we quantified deformation under combined internal pressure and axial displacement, revealing a strong coupling between circumferential and longitudinal stretches and

marked changes in curvature. This experimental framework lays essential groundwork for future biomechanical modeling of insect respiratory systems. It offers a new avenue for understanding how structural geometry influences function under complex *in vivo* loading conditions.

Acknowledgements

This research was supported by the National Science Foundation under Grant No. #0938047.

Competing interests

The authors declare that they have no competing interests.

Contribution

M. W. and R. D. conceived and designed the study, conducted the experiments, analyzed the data, and wrote the manuscript. R. W. assisted with data visualization. J. S. contributed expertise in insect physiology and assisted in manuscript preparation. All authors approved the final version of the manuscript for submission.

Funding

This work was supported by the National Science Foundation under grants No.# 0938047.

Data availability

The data supporting the findings of this study are available on GitHub at https://github.com/devitaraffaella/insect-tracheal-tube-inflation-data.

References

Aboelkassem, Y. and Staples, A.. (2012) Flow transport in a microchannel induced by moving wall contractions: A novel micropumping mechanism. *Acta Mech.* **223**, 463–480.

Appel, E., Michels, J., and Gorb, S.N. (2024) Resilin in insect flight systems. *Adv. Funct. Mater.* **34**(35), 2215162.

Becker, W. R., Webster, M. R., Socha, J. J., and De Vita, R. (2015) Variation in the mechanical properties of tracheal tubes in the American cockroach. *Smart Mater. Struct.* **14**, 549-560.

Chatterjee, K., Graybill, P. M., Socha, J. J., Davalos, R. V., and Staples, A. E. (2021) Frequency-specific, valveless flow control in insect-mimetic microfluidic devices. *Bioinspir. Biomim.* **16**(3), 036004.

Dorfmann, A., Trimmer, B. A., and Woods, W. A. (2007) A constitutive model for muscle properties in a soft-bodied arthropod. *J. R. Soc. Interface* **4**(13), 257–269.

Dorfmann, A. L., Woods, W. A., and Trimmer, B. A. (2008) Muscle performance in a soft-bodied terrestrial crawler: Constitutive modelling of strain-rate dependency. *J. R. Soc. Interface* **5**(20), 349–362.

Eberl, C., Gianola, D. S., and Thompson, R. Digital Image Correlation and Tracking. *Matlab Central, online database. www.mathworks.com/matlabcentral/fileexchange/loadFile.do*.

Garcia, D., Orteu, J. J., and Penazzi, L. (2002) A combined temporal tracking and stereo-correlation technique for accurate measurement of 3D displacements: application to sheet metal forming. *J. Mater. Process. Technol.* **125**, 736–742.

Gorpas, D., Politopoulos, K., and Yova, D. (2007) A binocular machine vision system for three-dimensional surface measurement of small objects. *Comput. Med. Imaging Graph.* **31**(8), 625–637.

Greenlee, K. J., Socha, J. J., Eubanks, H. B., Pedersen, P., Lee, W. K., and Kirkton, S. D. (2013) Hypoxia-induced compression in the tracheal system of the tobacco hornworm caterpillar, Manduca sexta. *J. Exp. Biol.* **216**(12), 2293–2301.

Harrison, J. F. (1997) Ventilatory mechanism and control in grasshoppers. *Integr. Comp. Biol.* **37**(1), 73.

Harrison, J. F. (2009) Tracheal system. In *Encyclopedia of Insects*, pp. 1011–1015. Elsevier.

Hartley, R., and Zisserman, A. (2000) *Multiple View Geometry in Computer Vision*, vol. 2. Cambridge Univ. Press.

Haughton, D. M., and Ogden, R. W. (1979) Bifurcation of inflated circular cylinders of elastic material under axial loading I. Membrane theory for thin-walled tubes. *J. Mech. Phys. Solids* **27**(3), 179–212.

Hepburn, H. R. (1972) Some mechanical properties of crossed fibrillar chitin. *J. Insect Physiol.* **18**(5), 815–825.

Hepburn, H. R., and Chandler, H. D. (1976a) Material properties of arthropod cuticles: The arthrodial membranes. *J. Comp. Physiol.* **109**(2), 177–198.

Hepburn, H. R., and Chandler, H. D. (1976b) Mechanical hysteresis of insect cuticles. *J. Insect Physiol.* **22**(2), 221–226.

Hochgraf, J. S., Waters, J. S., and Socha, J. J. (2018) Patterns of tracheal compression in the thorax of the ground beetle, *Platynus decentis*. *Yale J. Biol. Med.* **91**(4), 409.

Holzapfel, G. A., and Weizsäcker, H. W. (1998) Biomechanical behavior of the arterial wall and its numerical characterization. *Comput. Biol. Med.* **28**(4), 377–392.

Holzapfel, G. A., Gasser, T. C., and Ogden, R. W. (2000) A new constitutive framework for arterial wall mechanics and a comparative study of material models. *J. Elasticity Phys. Sci. Solids* **61**, 1–48.

Jensen, M., and Weis-Fogh, T. (1962) Biology and physics of locust flight. V. Strength and elasticity of locust cuticle. *Philos. Trans. R. Soc. Lond. B Biol. Sci.* **245**(721), 137–169.

Khan, S., and Staples, A. E. (2025) Mechanisms of insect respiration. *Nat. Rev. Phys.*, 1–14.

Kresch, E. (1977) Cross-sectional shape of flexible tubes. *Bull. Math. Biol.* **39**(6), 679–691.

Lin, H. T., Dorfmann, A. L., and Trimmer, B. A. (2009) Soft-cuticle biomechanics: A constitutive model of anisotropy for caterpillar integument. *J. Theor. Biol.* **256**(3), 447–457.

Matsumura, Y., Kovalev, A., and Gorb, S. N. (2021) Mechanical properties of a female reproductive tract of a beetle and implications for penile penetration. *Proc. R. Soc. B* **288**(1954), 20211125.

Miller, P. L. (1966) The supply of oxygen to the active flight muscles of some large beetles. *J. Exp. Biol.* **45**(2), 285–304.

Nguyen, V., Lilly, B., and Castro, C. (2014) The exoskeletal structure and tensile loading behavior of an ant neck joint. *J. Biomech.* **47**(2), 497–504.

Pendar, H., Aviles, J., Adjerid, K., Schoenewald, C., and Socha, J. J. (2019) Functional compartmentalization in the hemocoel of insects. *Sci. Rep.* **9**(1), 6075.

Ren, L., Li, B., Wei, G., Wang, K., Song, Z., Wei, Y., Ren, L., and Liu, Q. (2021) Biology and bioinspiration of soft robotics: Actuation, sensing, and system integration. *iScience* **24**(9).

Reynolds, S. E. (1975) The mechanical properties of the abdominal cuticle of *Rhodnius* larvae. *J. Exp. Biol.* **62**(1), 69.

Shan, Y., Philen, M. P., Bakis, C. E., Wang, K. W., and Rahn, C. D. (2006) Nonlinear-elastic finite axisymmetric deformation of flexible matrix composite membranes under internal pressure and axial force. *Compos. Sci. Technol.* **66**(15), 3053–3063.

Siamantouras, E., Woodrow, C., Celiker, E., Cullen, D. A., Hills, C. E., Squires, P. E., and Montealegre-Z, F. (2022) Quantification of bush-cricket acoustic trachea mechanics using atomic force microscopy nanoindentation. *Acta Biomater.* **153**, 399–410.

Smith, C. W., Herbert, R., Wootton, R. J., and Evans, K. E. (2000) The hind wing of the desert locust (*Schistocerca gregaria* Forskal). II. Mechanical properties and functioning of the membrane. *J. Exp. Biol.* **203**(19), 2933–2943.

Socha, J. J., Lee, W., Harrison, J. F., Waters, J. S., Fezzaa, K., and Westneat, M. W. (2008) Correlated patterns of tracheal compression and convective gas exchange in a carabid beetle. *J. Exp. Biol.* **211**, 3409.

Stamm, K., Saltin, B. D., and Dirks, J.-H. (2021) Biomechanics of insect cuticle: An interdisciplinary experimental challenge. *Appl. Phys. A* **127**(5), 329.

Suarez, R. K. (2000) Energy metabolism during insect flight: Biochemical design and physiological performance. *Physiol. Biochem. Zool.* **73**(6), 765–771.

Takamizawa, K., and Hayashi, K. (1987) Strain energy density function and uniform strain hypothesis for arterial mechanics. *J. Biomech.* **20**(1), 7–17.

Vangerko, H., and Treloar, L. R. G. (1978) The inflation and extension of rubber tube for biaxial strain studies. *J. Phys. D Appl. Phys.* **11**(14), 1969.

Vincent, J. F. V., and Wegst, U. G. K. (2004) Design and mechanical properties of insect cuticle. *Arthropod Struct. Dev.* **33**(3), 187–199.

Webster, M. R., De Vita, R., Twigg, J. N., and Socha, J. J. (2011) Mechanical properties of tracheal tubes in the American cockroach (*Periplaneta americana*). *Smart Mater. Struct.* **20**, 094017.

Webster, M. R., Socha, J. J., Teresi, L., Nardinocchi, P., and De Vita, R. (2015a) Structure of tracheae and the functional implications for collapse in the American cockroach. *Bioinspir. Biomim.* **10**(6), 066011.

Webster, M. R. (2015b) Mechanical characterization of insect tracheal tubes. *Ph.D. Dissertation, Virginia Tech*.

Weis-Fogh, T. (1960) A rubber-like protein in insect cuticle. *J. Exp. Biol.* **37**(4), 889–907.

Weis-Fogh, T. (1967) Respiration and tracheal ventilation in locusts and other flying insects. *J. Exp. Biol.* **47**(3), 561–587.

Westneat, M. W., Betz, O., Blob, R. W., Fezzaa, K., Cooper, W. J., and Lee, W. K. (2003) Tracheal respiration in insects visualized with synchrotron X-ray imaging. *Science* **299**(5606), 558.

Westneat, M. W., Socha, J. J., and Lee, W. K. (2008) Advances in biological structure, function, and physiology using synchrotron X-ray imaging. *Physiology* **70**(1), 119.

Wicker, B. K., Hutchens, H. P., Wu, Q., Yeh, A. T., and Humphrey, J. D. (2008) Normal basilar artery structure and biaxial mechanical behaviour. *Comput. Methods Biomech. Biomed. Eng.* **11**(5), 539–551.

Williams, C. M. (1946) Physiology of insect diapause: the role of the brain in the production and termination of pupal dormancy in the giant silkworm, *Platysamia cecropia*. *Biol. Bull.* **90**(3), 234–243.

Zheng, Y., Wang, J., Wang, J., Li, Y., and Jiang, Z. (2025) Insect cuticle: A source of inspiration for biomimetic interface material design. *Colloids Interface Sci. Commun.* **64**, 100818.

Figures

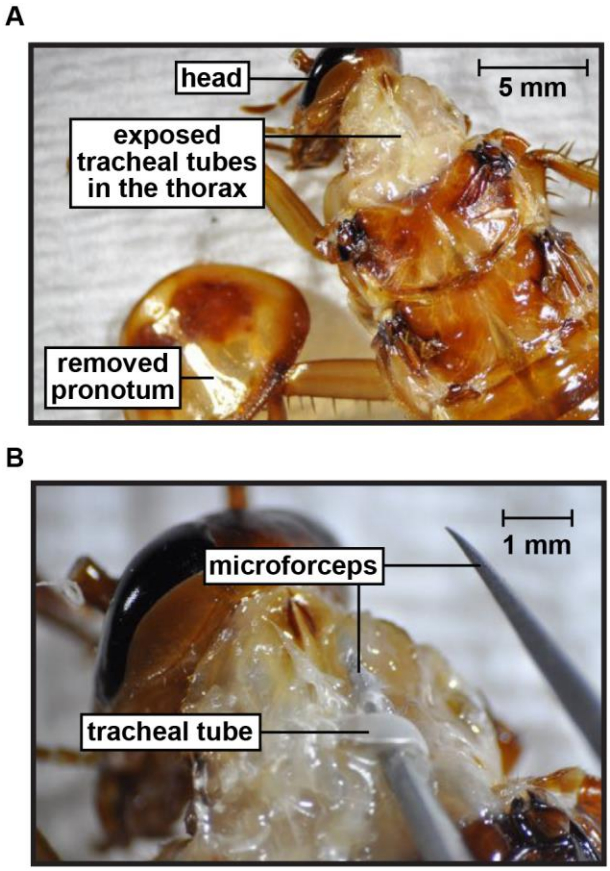

Fig. 1. Picture of the anatomy of the thoracic tracheal system in the American cockroach. **A.** Exposed thoracic cavity showing the tracheal network. **B.** Isolated primary tracheal tube within the thorax.

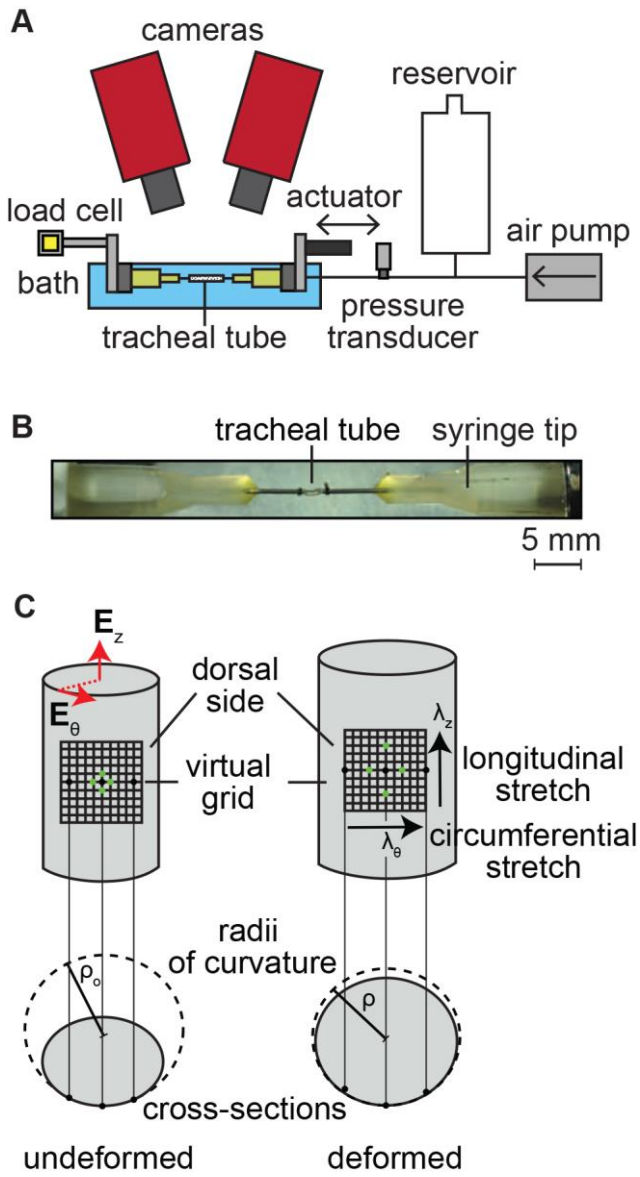

Fig. 2. Custom-built testing system developed for inflation-extension experiments on insect tracheal tubes, providing simultaneous measurement of longitudinal and circumferential stretches and radius of curvature. A. Schematic with the main components of testing system. **B.** Picture of an insect tracheal tube clamped between two syringe tips. **C.** Undeformed and deformed tracheal tube showing the virtual grid used to track deformations, including longitudinal stretch, λ_z, circumferential stretch, λ_θ, and radius of curvature, ρ. Green points represent corresponding virtual grid nodes used to calculate local stretches and curvature from tracked displacements. $\boldsymbol{E}_z$ and $\boldsymbol{E}_\theta$ are the two directions of loading: the longitudinal and circumferential directions.

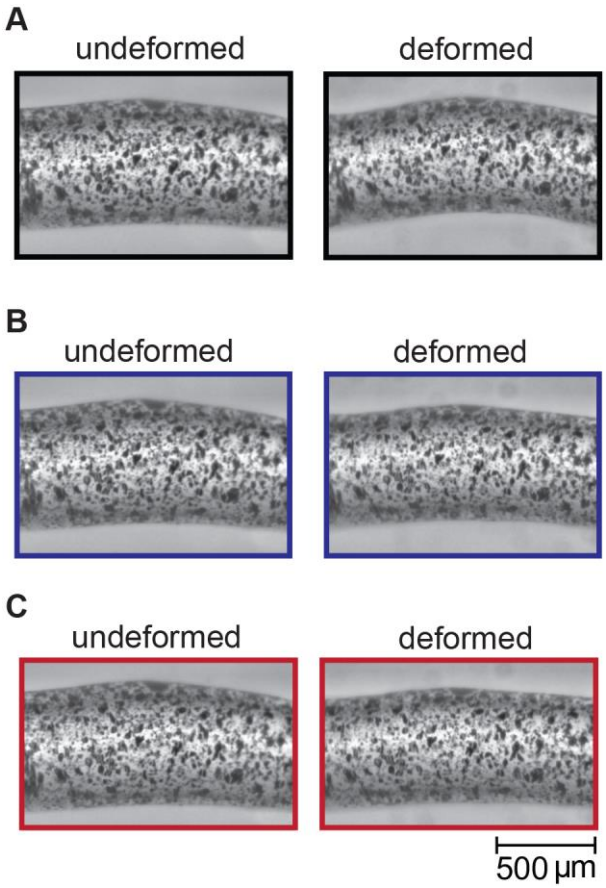

Fig. 3. Pictures of undeformed and deformed configurations to 6 kPa of a tracheal tube (speckle-coated for DIC) subjected to inflation at three axial displacements. A. $\delta_z = 0$ mm, **B.** $\delta_z = 0.1$ mm, and **C.** $\delta_z = 0.2$ mm.

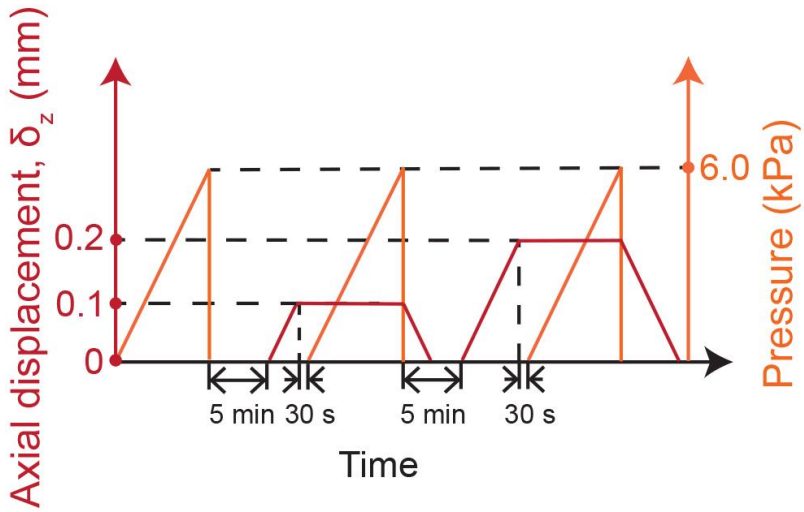

Fig. 4. Schematic of the inflation-extension test protocol used to test the insect tracheal tubes. Three inflation tests were conducted on each tracheal specimen at axial displacements δ_z of 0.0, 0.1, and 0.2 mm. Each specimen was allowed to relax for approximately 5 min between elongation levels. At each fixed displacement, the specimen was allowed to equilibrate for 30 s before being internally pressurized to a maximum of 6 kPa while circumferential and longitudinal stretches were measured.

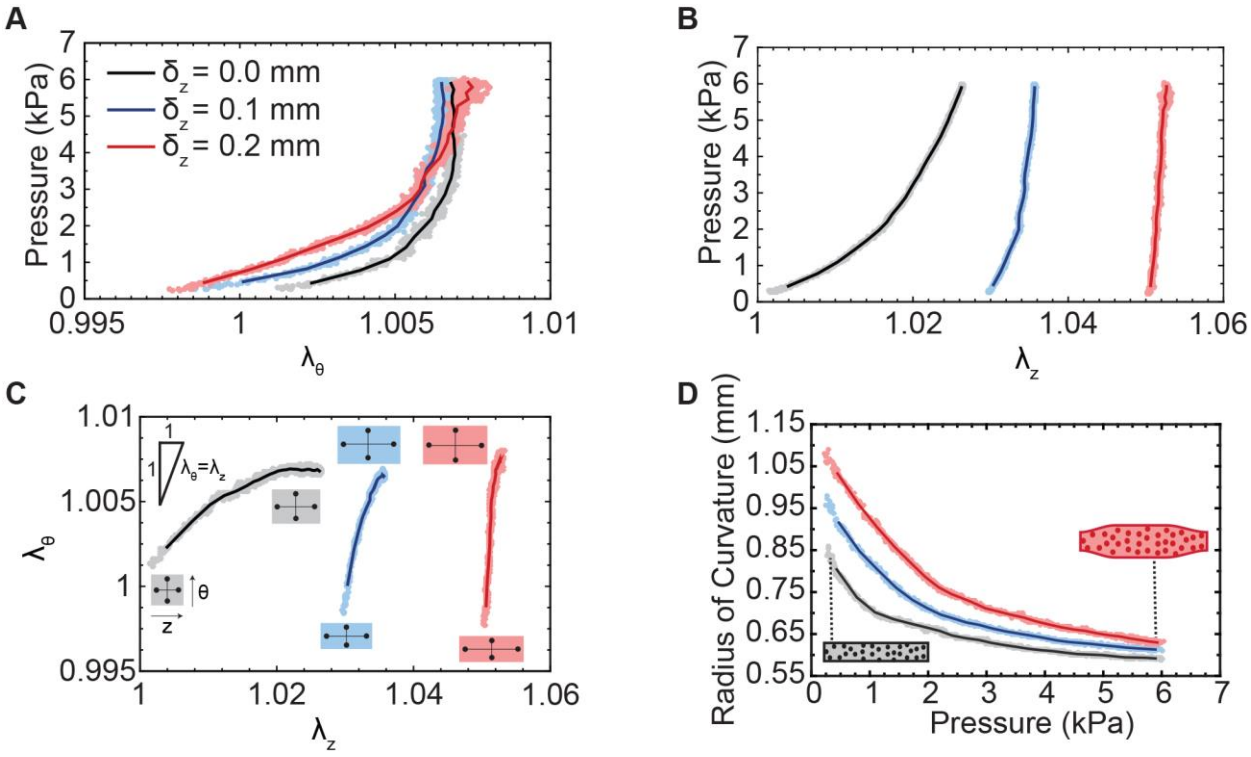

Fig. 5. Experimental results for a representative specimen (specimen 3 in Figs. 6-7). A. Internal pressure versus circumferential stretch λ_θ data. **B.** Internal pressure versus longitudinal stretch λ_z data. **C.** Longitudinal stretch λ_θ versus circumferential stretch λ_θ data. Inset schematics illustrate the local deformation of an initially square region on the tracheal surface. The square has one side in the circumferential direction (the θ-direction) and the other side in the longitudinal direction (the $z-$direction). Deformation of the square reflects local strain: circumferential expansion or contraction alters the vertical dimension while longitudinal elongation stretches the horizontal dimension. Insets are color-coded to match the corresponding axial displacement δ_z. The triangle indicates the isometric condition ($\lambda_\theta = \lambda_z$), corresponding to equal circumferential and longitudinal deformations. **D.** Radius of (circumferential) curvature versus pressure data, with schematic insets of the trachea before testing and after completion of the full protocol. Data are collected from one representative tracheal tube (specimen 3 in Figs. 6-7 subjected to inflation-extension tests at three axial displacements: $\delta_z = 0.0$, 0.1, and 0.2 mm. Individual data points are shown with semi-transparent markers; solid lines represent moving averages.

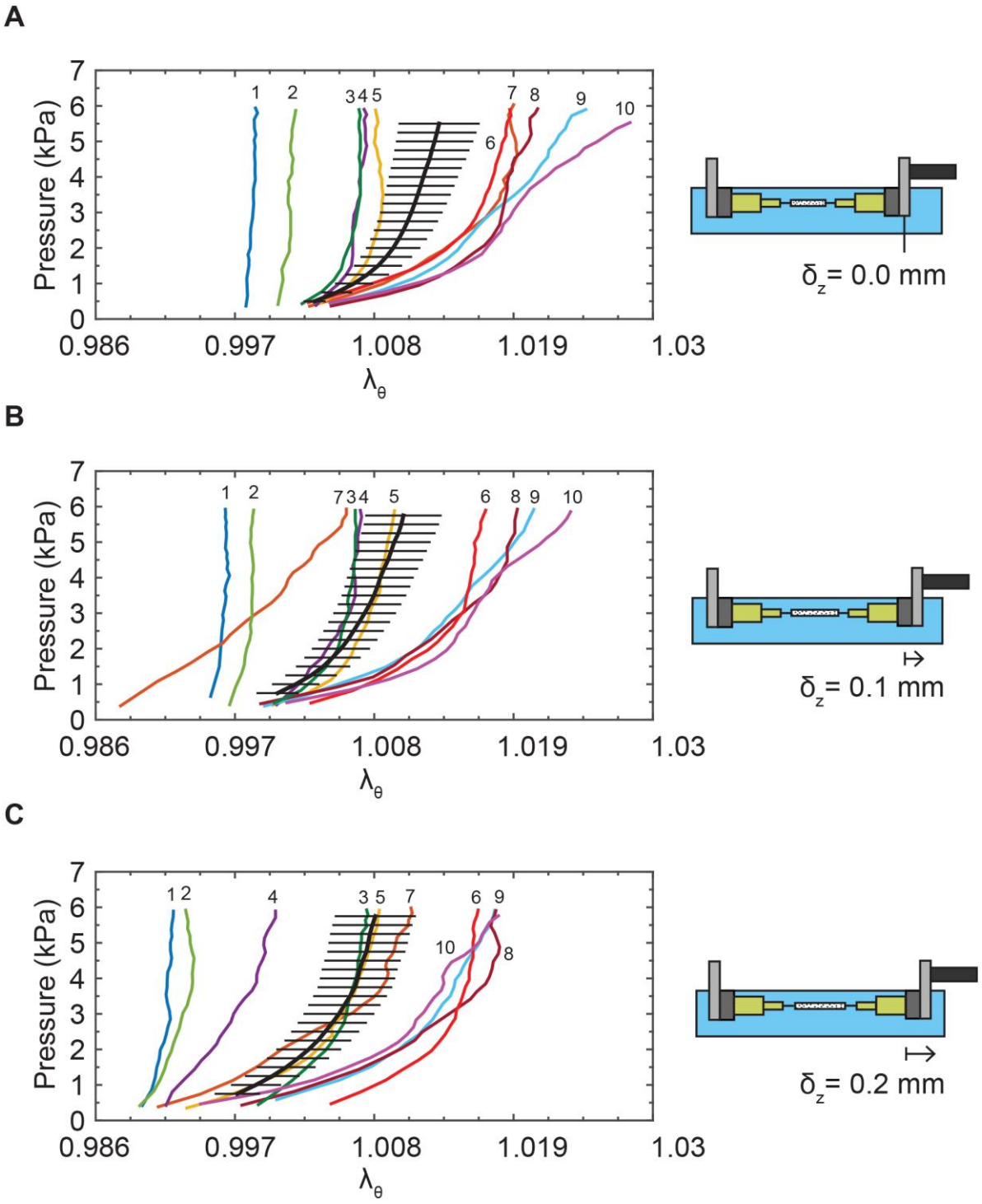

Fig. 6. Internal pressure versus circumferential stretch λ_θ data for n = 10 specimens at three axial displacements. A. $\delta_z = 0\,\text{mm}$, **B.** $\delta_z = 0.1\,\text{mm}$, and **C.** $\delta_z = 0.2\,\text{mm}$. Data for each specimen at different axial displacements δ_z are reported using the same color in A, B, and C. Mean (with S.E.M.) is reported in black.

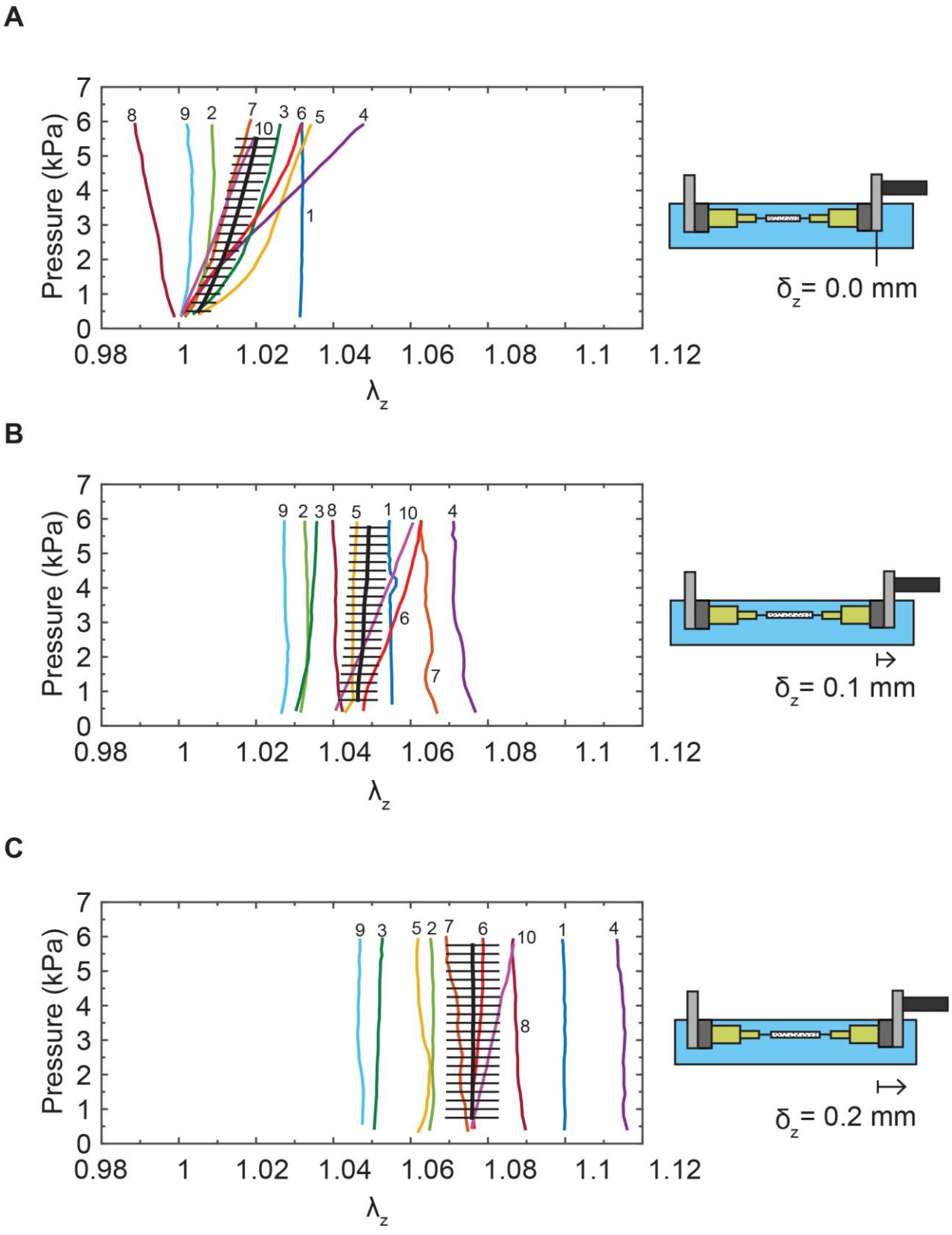

Fig. 7. Internal pressure versus longitudinal stretch λ_z data for n = 10 specimens at three axial displacements. A. $\delta_z = 0\,\text{mm}$, **B.** $\delta_z = 0.1\,\text{mm}$, and **C.** $\delta_z = 0.2\,\text{mm}$. Data for each specimen at different axial displacements δ_z are reported using the same color in A, B, and C. Mean (with S.E.M.) is reported in black.

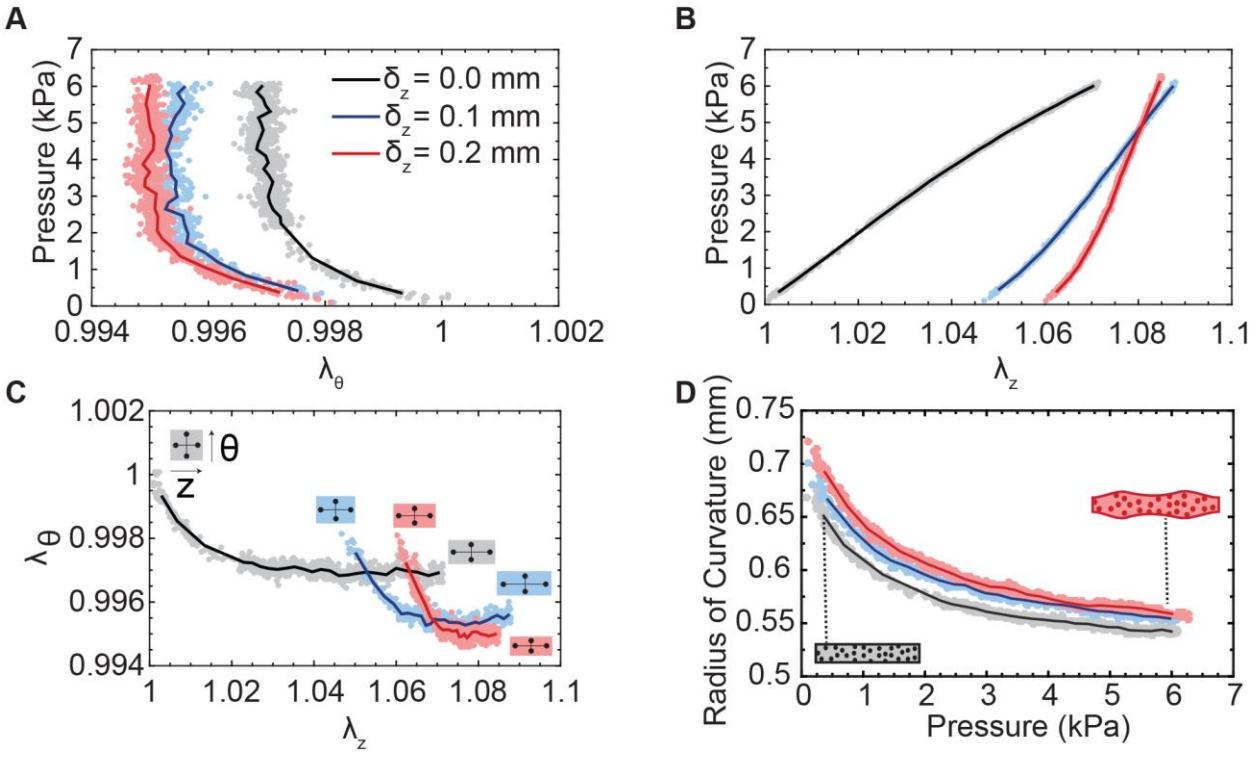

Fig. 8. Experimental results for a non-representative specimen. A. Internal pressure versus circumferential stretch λ_θ data. **B.** Internal pressure versus longitudinal stretch λ_z data. **C.** Longitudinal stretch λ_θ versus circumferential stretch λ_θ data. Inset schematics illustrate the local deformation of an initially square region on the tracheal surface. The square has one side in the circumferential direction (the θ-direction) and the other side in the longitudinal direction (the $z-$direction). Deformation of the square reflects local strain: circumferential contraction alters the vertical dimension while longitudinal elongation stretches the horizontal dimension. Insets are color-coded to match the corresponding axial displacement δ_z. **D.** Radius of (circumferential) curvature versus pressure data, with schematic insets of the trachea before testing and after completion of the full protocol. Data are collected from one representative tracheal tube subjected to inflation-extension tests at three axial displacements: $\delta_z = 0.0$, 0.1, and 0.2 mm. Individual data points are shown with semi-transparent markers; solid lines represent moving averages.